

TRPP2 and TRPV4 form a polymodal sensory channel complex

Michael Köttgen,¹ Björn Buchholz,¹ Miguel A. Garcia-Gonzalez,³ Fruzsina Kotsis,¹ Xiao Fu,¹ Mara Doerken,¹ Christopher Boehlke,¹ Daniel Steffl,¹ Robert Tauber,¹ Tomasz Wegierski,¹ Roland Nitschke,⁵ Makoto Suzuki,² Albrecht Kramer-Zucker,¹ Gregory G. Germino,³ Terry Watnick,³ Jean Prenen,⁴ Bernd Nilius,⁴ E. Wolfgang Kuehn,¹ and Gerd Walz¹

¹Renal Division, University Hospital Freiburg, 79106 Freiburg, Germany

²Department of Pharmacology, Jichi Medical School, Minamikawachi, Tochigi 329-0498, Japan

³Division of Nephrology, Department of Medicine, Johns Hopkins University School of Medicine, Baltimore, MD 21205

⁴Laboratory of Physiology, Katholieke Universiteit Leuven, B-3000 Leuven, Belgium

⁵Department of Developmental Biology, University of Freiburg, 79104 Freiburg, Germany

The primary cilium has evolved as a multifunctional cellular compartment that decorates most vertebrate cells. Cilia sense mechanical stimuli in various organs, but the molecular mechanisms that convert the deflection of cilia into intracellular calcium transients have remained elusive. Polycystin-2 (TRPP2), an ion channel mutated in polycystic kidney disease, is required for cilia-mediated calcium transients but lacks mechanosensitive properties. We find here that TRPP2 utilizes TRPV4 to form

a mechano- and thermosensitive molecular sensor in the cilium. Depletion of TRPV4 in renal epithelial cells abolishes flow-induced calcium transients, demonstrating that TRPV4, like TRPP2, is an essential component of the ciliary mechanosensor. Because TRPV4-deficient zebrafish and mice lack renal cysts, our findings challenge the concept that defective ciliary flow sensing constitutes the fundamental mechanism of cystogenesis.

Introduction

Primary cilia function as sensory organelles that detect a variety of chemical and physical stimuli. The cilia of renal epithelial cells are exposed to fluid flow that bends this microtubule-based organelle, eliciting an increase in intracellular calcium (Praetorius and Spring, 2001). The calcium transient is contingent on the presence of the polycystin-1–TRPP2 protein complex (Nauli et al., 2003). TRPP2, a member of the transient receptor potential (TRP) family of ion channels, assembles with the PKD1 gene product polycystin-1, a large integral membrane protein with distant homology to TRP channels, to form a receptor-ion channel complex (Hanaoka et al., 2000; Köttgen, 2007). Mutations in polycystin-1 or TRPP2 cause autosomal dominant polycystic kidney disease,

and deletion of either of the two proteins causes multiple developmental abnormalities in mice, most notably fluid-filled cysts in the kidney, liver, and pancreas (Lu and Zhou, 1997; Wu et al., 1998; Kim et al., 2000). How polycystin-1 and TRPP2 exert their diverse biological functions has remained largely unknown. Both proteins localize to the primary cilium but assume other distinct subcellular localizations that are regulated by multiple adaptor proteins (Hidaka et al., 2004; Köttgen and Walz, 2005). The flow-mediated Ca^{2+} transient requires the presence of functional TRPP2 (Nauli et al., 2003) and has been implicated in the regulation of tubular polarity and morphology. Because functional and structural defects of the primary cilium cause polycystic kidney disease, it is currently widely accepted that the loss of tubular flow sensing constitutes the fundamental mechanism of cystogenesis (Ong and Wheatley, 2003; Torres and Harris, 2006). Although the localization and calcium permeability of TRPP2 make it an attractive candidate for the ciliary calcium entry pathway, the homomeric channel lacks mechanosensitivity (Giamarchi et al., 2006).

M. Köttgen and B. Buchholz contributed equally to this paper.

Correspondence to Wolfgang Kuehn: wolfgang.kuehn@uniklinik-freiburg.de; or Gerd Walz: gerd.walz@uniklinik-freiburg.de

M. Köttgen's present address is Department of Biological Chemistry, Johns Hopkins School of Medicine, Baltimore, MD 21205.

B. Buchholz's present address is Department of Nephrology, Friedrich-Alexander University, 91054 Erlangen, Germany

Abbreviations used in this paper: FRET, fluorescence resonance energy transfer; hpf, hours postfertilization; MO, morpholino oligonucleotide; RR, ruthenium red; TRP, transient receptor potential.

The online version of this paper contains supplemental material.

© 2008 Köttgen et al. This article is distributed under the terms of an Attribution-Noncommercial-Share Alike-No Mirror Sites license for the first six months after the publication date (see <http://www.jcb.org/misc/terms.shtml>). After six months it is available under a Creative Commons License (Attribution-Noncommercial-Share Alike 3.0 Unported license, as described at <http://creativecommons.org/licenses/by-nc-sa/3.0/>).

Thus, we hypothesized that TRPP2 assembles with an auxiliary subunit to form a mechanosensitive channel complex.

Results and discussion

TRPV4 localizes to the cilium and interacts with TRPP2

In *Caenorhabditis elegans*, the TRPV channel OSM-9 is involved in transmitting multiple sensory stimuli, including olfaction, osmosensation, and mechanosensation. Specificity is provided by interaction with specific OSM-9 and capsaicin receptor-related (OCR) ion channels, and signaling depends on the correct targeting of these ion channels to the cilium of sensory neurons (Tobin et al., 2002; Kahn-Kirby and Bargmann, 2006). Because human TRPV4 is related to OSM-9, rescues the avoidance defects of OSM-9-deficient worms in response to hyperosmotic stress and nose touch (Liedtke et al., 2003), and is expressed in the kidney (Tian et al., 2004) as well as the zebrafish pronephros (Mangos et al., 2007), we postulated that TRPV4 may access the ciliary compartment in the kidney of vertebrates. Recently, TRPV4 was found in cilia in cholangiocytes and the oviduct (Teilmann et al., 2005; Gradiolone et al., 2007). Consistent with its expression pattern in *C. elegans* and these mammalian tissues, TRPV4 localized to the cilia of polarized MDCK cells, where it colocalized with TRPP2 (Fig. 1, A–D; and Fig. S1, available at <http://www.jcb.org/cgi/content/full/jcb.200805124/DC1>). Accordingly, we investigated whether TRPV channels are involved in flow-mediated calcium signaling and found that flow-triggered calcium transients in ciliated MDCK cells were completely abrogated by 500 nM of the polycationic ruthenium red (RR), a compound that inhibits TRPV channels (Fig. S2; Voets et al., 2002). These observations led us to speculate that TRPP2 may interact with TRPV4 to mediate tissue-specific functions such as ciliary mechanosensation.

Because TRP channels are known to engage in heteromeric interactions that generate channels with novel functional properties (Schaefer, 2005), we tested whether TRPP2 physically interacts with TRPV4. As shown in Fig. 1 E, the carboxy terminus of TRPP2 immunoprecipitated wild-type TRPV4 as well as the carboxy terminus of TRPV4 (Fig. 1 F). Conversely, precipitation of the carboxy terminus of TRPV4 immobilized wild-type TRPP2 (Fig. 1 G). To confirm these coimmunoprecipitation assays, we used fluorescence resonance energy transfer (FRET) to test whether the carboxy-terminal domains of TRPP2 and TRPV4 associate within living cells. As shown in Fig. 1 (H–J), fusion of CFP and YFP to full-length TRPP2 and TRPV4, respectively, resulted in FRET, which provides further evidence that TRPP2 and TRPV4 form heteromultimers. FRET was not observed when using TRPC6-YFP as a negative control (Fig. S1, G–I).

Functional interaction between TRPP2 and TRPV4

To study whether TRPP2 and TRPV4 also interact functionally, we expressed both channels in *Xenopus laevis* oocytes for electrophysiological analysis. TRPV4 is activated by a variety of stimuli, including hypotonicity-induced cell swelling, which is akin to a mechanical stimulus (Liedtke et al., 2000; Nilius et al., 2001, 2004).

Because a carboxy-terminal acidic cluster precludes the expression of TRPP2 at the cell surface (Köttgen et al., 2005), only TRPV4, but not TRPP2, raised the steady-state inward currents in *X. laevis* oocytes. Hypotonic cell swelling further increased TRPV4 currents (Fig. 2 A). Coexpression of TRPV4 and TRPP2 significantly augmented the swelling-activated currents in *X. laevis* oocytes, whereas steady-state currents remained unchanged (Fig. 2 A). The swelling-induced conductance was more than doubled in TRPV4/TRPP2-expressing cells in comparison with TRPV4-expressing cells (Fig. 2 B). Neither water nor TRPP2-injected oocytes showed any swelling-activated currents (Fig. 2, A and B). The current–voltage relationship revealed a slight outward rectification of the TRPV4 currents that was not substantially influenced by coexpression of TRPP2 (Fig. 2, C and D). Increasing the extracellular Ca²⁺ concentration led to a significant increase in whole-cell currents in TRPV4-expressing oocytes. This effect was dramatically augmented in oocytes coexpressing TRPP2 (Fig. 2, E and F). Thus, TRPP2 alters the functional properties of TRPV4. We also observed a functional interaction between TRPP2 and TRPV4 in HEK 293 cells (Fig. S3, available at <http://www.jcb.org/cgi/content/full/jcb.200805124/DC1>). To address the question of whether the TRPP2 effect on swelling-activated currents is simply mediated through increased surface expression of TRPV4, we inserted a V5 tag into the first extracellular loop of TRPV4 and TRPP2, respectively, and monitored either ion channel at the cell surface using a modified ELISA system (Wegierski et al., 2006). Interestingly, coexpression of TRPV4 significantly increased TRPP2 surface expression (Fig. 2 G), whereas TRPP2 reduced both TRPV4 surface expression and TRPV4 total protein levels (Fig. 2 I). Thus, the increases in swelling-induced conductance are not the result of increased TRPV4 surface expression but rather caused by altered channel properties through formation of TRPP2/TRPV4 heteromers.

These findings demonstrate that TRPP2 and TRPV4 physically and functionally interact, thereby raising the question of whether TRPP2 nonspecifically alters the activity of TRP channels in vitro. TRPP2 is known to interact with TRPC1 (Tsiokas et al., 1999); therefore, we tested whether TRPP2 influences the channel properties of TRPC1 in *X. laevis* oocytes. TRPP2 did not alter the whole cell currents mediated by expression of TRPC1 (unpublished data), which indicates that physical interaction with TRPP2 alone does not suffice to alter the functional properties of another TRP channel, at least under the experimental conditions used here.

TRPV4 is an essential component of the ciliary flow sensor in MDCK cells

Calcium transients, triggered by ciliary bending, were first established in MDCK cells (Praetorius and Spring, 2001) and then subsequently validated in other in vitro and in vivo systems (Nauli et al., 2003; Liu et al., 2005). To test whether TRPV4 is a component of the flow sensor in the primary cilium, we studied flow-induced Ca²⁺ transients in MDCK cells. We used a lentiviral siRNA approach to inducibly knock down endogenous TRPV4. After identifying two siRNA oligonucleotides that efficiently reduced expression of canine TRPV4 (Fig. 3 A), we generated polyclonal MDCK cells expressing TRPV4 siRNA under

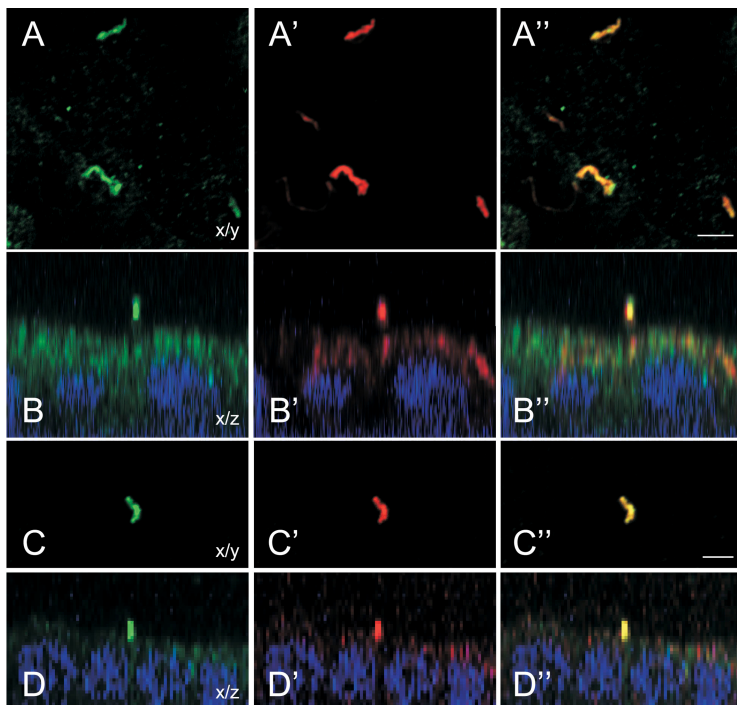
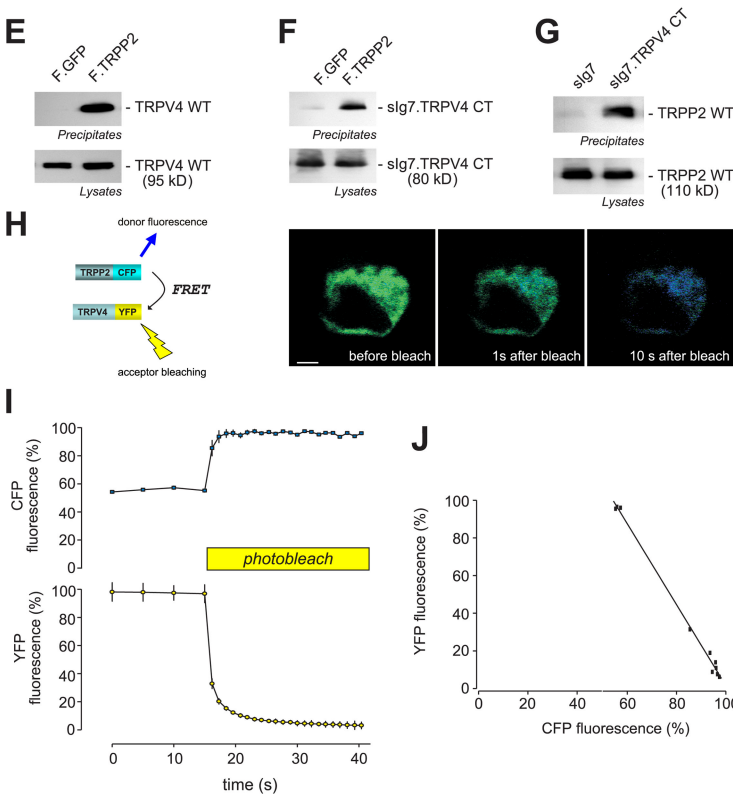


Figure 1. TRPV4 and TRPP2 interact and colocalize in primary cilia. (A) Subcellular localization of native TRPV4 and TRPP2 in polarized MDCK cells. TRPV4 localizes to primary cilia. Confocal images were acquired at the level of the apical membrane. TRPV4 (A) and acetylated tubulin (A') colocalize in the primary cilium (A'': merge). (B) Confocal z sections show that the primary cilium emerges from the apical membrane (B: anti-TRPV4; B': anti-acetylated tubulin; B'': merge). (C) TRPV4 and TRPP2 (C') colocalize in the primary cilium (C'': merge). (D) z section of a confocal image z stack of the cells shown in C. (E) Coimmunoprecipitation of TRPP2 and TRPV4 in HEK 293 cells. The flag-tagged carboxy terminus of TRPP2 (F.TRPP2) coprecipitates wild-type TRPV4, and the carboxy terminus of TRPV4 fused to a membrane-anchored immunoglobulin tag (slg7.TRPV4 CT; F). (G) The same TRPV4 fusion protein precipitates TRPP2 wild type (WT). (H) FRET between TRPP2-CFP and TRPV4-YFP was revealed by increase in donor fluorescence after acceptor bleaching. HEK 293 cells were transfected with TRPP2-CFP and TRPV4-YFP. TRPP2-CFP was excited at 458 nm, and the emitted CFP and YFP fluorescence was recorded before and after photobleaching of the YFP fluorescence at 488 nm. (I) Time course of the normalized CFP and YFP fluorescence during photobleaching experiments ($n = 5$). (J) Correlation of the relative amount of YFP photobleaching and the concomitant increase in CFP fluorescence in the same cell. Bars, 5 μ m.



the control of the TET repressor; the expression of siRNA in individual cells was monitored by the concomitant expression of GFP (Fig. 3, B and C). Ciliary bending was achieved by superfusing ciliated MDCK cells at physiological flow rates in a laminar flow chamber (Praetorius and Spring, 2001; Kotsis et al., 2007). Noninduced MDCK cells did not express TRPV4 siRNA and consistently displayed Ca^{2+} signals upon flow stimulation like wild-type MDCK cells (Fig. 3, B, D, and F). However,

flow-induced Ca^{2+} signals were virtually abolished in the same cells after the induction of TRPV4 siRNA expression by tetracycline (Fig. 3, C, E, G, and H). MDCK cells expressing the second TRPV4 siRNA construct showed similar results, whereas GFP- and siRNA-negative cells displayed the typical, flow-induced Ca^{2+} signals (unpublished data). Furthermore, robust flow-induced Ca^{2+} signals were observed in MDCK cells expressing a TRPV4 siRNA with a two-base mismatch, which

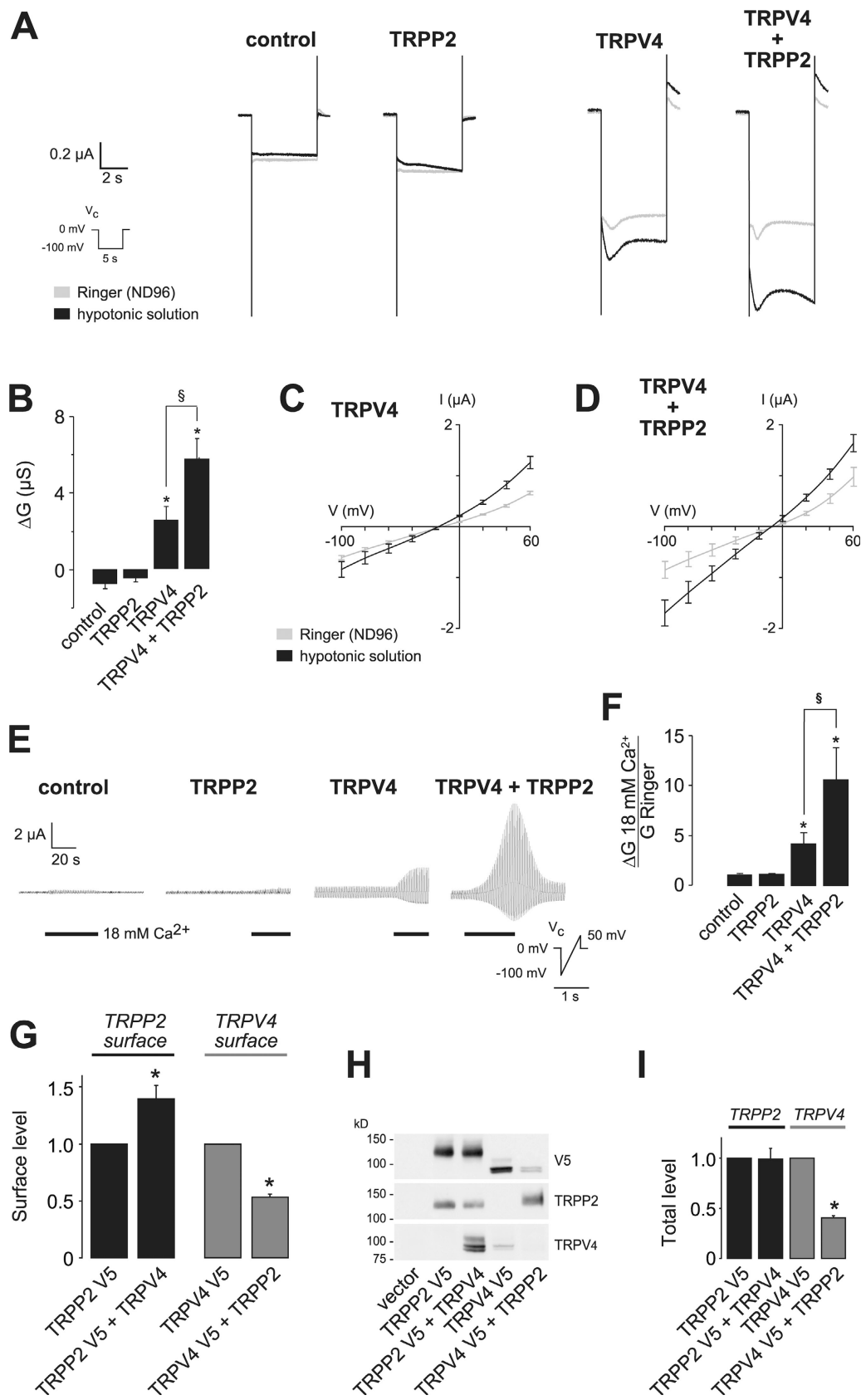


Figure 2. Functional interaction of TRPP2 and TRPV4 in *X. laevis* oocytes. (A) Analysis of TRP channel whole-cell currents under voltage clamp (V_c) conditions. Currents were recorded in *X. laevis* oocytes injected with cRNA encoding TRPP2 and/or TRPV4. Mean currents in Ringer or hypotonic solution are shown. (B) Summary of data acquired in A. Asterisks indicate significant differences in the hypotonicity-induced whole-cell conductance (ΔG) compared with water-injected control oocytes; §, significant difference between bars as indicated ($n = 21, 15, 38$, and 37 , respectively). (C and D) Current-voltage (I - V) relations for oocytes expressing TRPV4 or TRPV4 and TRPP2 (D; $n = 7$). (E) Increasing the extracellular Ca^{2+} concentration from 1.8 to 18 mM

does not alter TRPV4 expression levels (Fig. S2, G–I). These results demonstrate that TRPV4 is an essential component of the ciliary flow sensor in MDCK cells.

Role of TRPP2 and TRPV4 in cystogenesis

TRPV4-deficient mice display defective osmoregulation and thermosensation but fail to develop polycystic kidney disease (Liedtke and Friedman, 2003; Mizuno et al., 2003; Lee et al., 2005). We never observed cystic kidneys in TRPV4-deficient mice up to an age of 12 mo ($n = 10$). To investigate the role of TRPV4 in another animal model for cystogenesis, we studied the development of the pronephros during early zebrafish embryogenesis. Microinjection of a morpholino oligonucleotide (MO) directed against Zebrafish TRPP2 (pkd2MO) induces pronephric cysts that are detectable 48 h postfertilization (hpf; Fig. 4, A and B; Sun et al., 2004; Obara et al., 2006). However, neither injection of trpv4MO (Fig. 4, C and E) nor coinjection of trpv4MO in combination with low concentrations of pkd2MO resulted in a significant increase in cyst formation in the zebrafish pronephros (Fig. 4, D and F). The zebrafish results are consistent with the lack of renal cysts in the TRPV4-deficient mice, which suggests that TRPV4, although an essential component of the ciliary mechanosensor in MDCK cells in vitro, does not play an important role in cystogenesis in mouse or zebrafish. The question then arises of whether there is any evidence that TRPV4 is required for flow-induced calcium transients in vivo. Flow-dependent potassium secretion is a calcium-dependent process that is completely abolished in TRPV4 knockout mice (Taniguchi et al., 2007). These findings strongly suggest that flow-induced calcium transients are absent in at least the distal nephrons of adult TRPV4-deficient mice and question the importance of flow-mediated calcium signaling in cystogenesis. We cannot exclude the possibility that flow sensing plays a role in regulating tubular morphology during embryonic development. Yet, to our knowledge, there is no direct experimental evidence supporting a role for flow sensing during development because the role of polycystin-1 and TRPP2 was also studied in cell lines (Nauli et al., 2003).

The TRPP2-TRPV4 complex functions as a thermosensor in vivo

Given the lack of epistasis between TRPP2 and TRPV4 in the zebrafish pronephros model, we chose another approach to investigate whether TRPP2 and TRPV4 form a sensory complex in vivo. TRPV4 is activated by warm temperature in addition to osmotic stress (Guler et al., 2002; Watanabe et al., 2002). TRPV4-deficient mice exhibit reduced responses to noxious stimuli and inflammation-induced thermal hyperalgesia (Liedtke

and Friedman, 2003; Mizuno et al., 2003; Suzuki et al., 2003; Todaka et al., 2004), as well as a defective avoidance behavior at temperatures between 45 and 46°C, but a normal thermosensation profile at temperatures $\geq 47^\circ\text{C}$ (Lee et al., 2005). To test whether TRPV4 and TRPP2 form a complex that is activated by warm temperatures, we expressed both proteins in *X. laevis* oocytes. The activation of TRPV4 by warm temperatures (39°C) was doubled in the presence of TRPP2 (Fig. 5, A–D), which is consistent with the hypothesis that the TRPV4–TRPP2 channel complex exerts a thermosensory function. Using a tail immersion assay, we detected that TRPP2^{+/−} mice display a thermosensation profile that closely resembles the abnormalities described for TRPV4^{−/−} mice (Fig. 5, E and F). Latencies in the tail immersion assay were significantly increased at 44°C and 46°C in TRPP2^{+/−} mice (Fig. 5 E) but were comparable to wild-type mice at higher temperatures (Fig. 5 F). No differences were detected between wild-type and TRPV4^{+/−} mice; however, the additional loss of one TRPP2 allele (transheterozygous animals) drastically augmented the thermosensory defect at 44°C and 46°C, exceeding the latencies for either TRPV4^{−/−} or TRPP2^{+/−} mice (Fig. 5, E and F). These findings provide clear genetic evidence that TRPV4 and TRPP2 collectively mediate thermosensation at moderately warm temperatures in the mouse. Our findings demonstrate that TRPP2 and TRPV4 jointly mediate thermosensation at moderate temperatures. Recent observations strongly support the concept that basal body and ciliary proteins play a role in temperature sensation, providing a link between the subcellular localization and function of the ion channels studied here (Tan et al., 2007).

Although many TRP channels form heteromers, the physiological relevance of most interactions is poorly understood. Using progressively complex model systems, we demonstrate that coupling between two TRP channels, TRPP2 and TRPV4, creates a polymodal sensory channel complex, both in vitro and in vivo. Because TRPP2 is expressed in nearly all tissues, our results point toward a mechanism by which TRPP2 promiscuously exploits other TRP channel members to exert tissue-specific functions. This mechanism is also used by *C. elegans*, where OSM-9 provides the multifunctional TRP channel subunit that mediates responses to different sensory stimuli. It is tempting to speculate that TRPP2 utilizes TRPV4 to mediate mechano- and osmosensory signals required for TRPP2 functions such as systemic osmotic and blood pressure regulation that are impaired in polycystic kidney disease before the onset of renal failure. This hypothesis is supported by the recent finding that TRPV4 may also play a role in shear stress detection besides its role as an osmosensor (Wu et al., 2007). Although both channels localize to the cilium of tubular epithelial cells and are required

led to a significant increase in whole-cell currents in TRPV4-expressing oocytes. This effect was dramatically augmented in oocytes coexpressing TRPP2. Currents were continuously monitored under voltage clamp conditions (V_c protocol as indicated). (F) Analysis of the relative Ca^{2+} conductance revealed that TRPP2 significantly increased the Ca^{2+} currents (normalized group data, $G_{\text{Ca}}^{2+}/G_{\text{Ringer}}$ from E; $n = 10, 10, 11$, and 7, respectively). Whole-cell currents of oocytes expressing TRPV4 with or without TRPP2 were inhibited by RR with similar potency (see Fig. S2, available at <http://www.jcb.org/cgi/content/full/jcb.200805124/DC1>). (G) Analysis of the surface expression of TRPP2 and TRPV4 ($n = 4$) using an enzyme-linked assay for detection of both channels at the plasma membrane. Asterisks indicate significant differences between black and grey bars, respectively. (H) Representative Western blot of total protein amount of a representative experiment. (I) Summarized data of total protein amounts ($n = 4$). Error bars represent mean values \pm SEM.

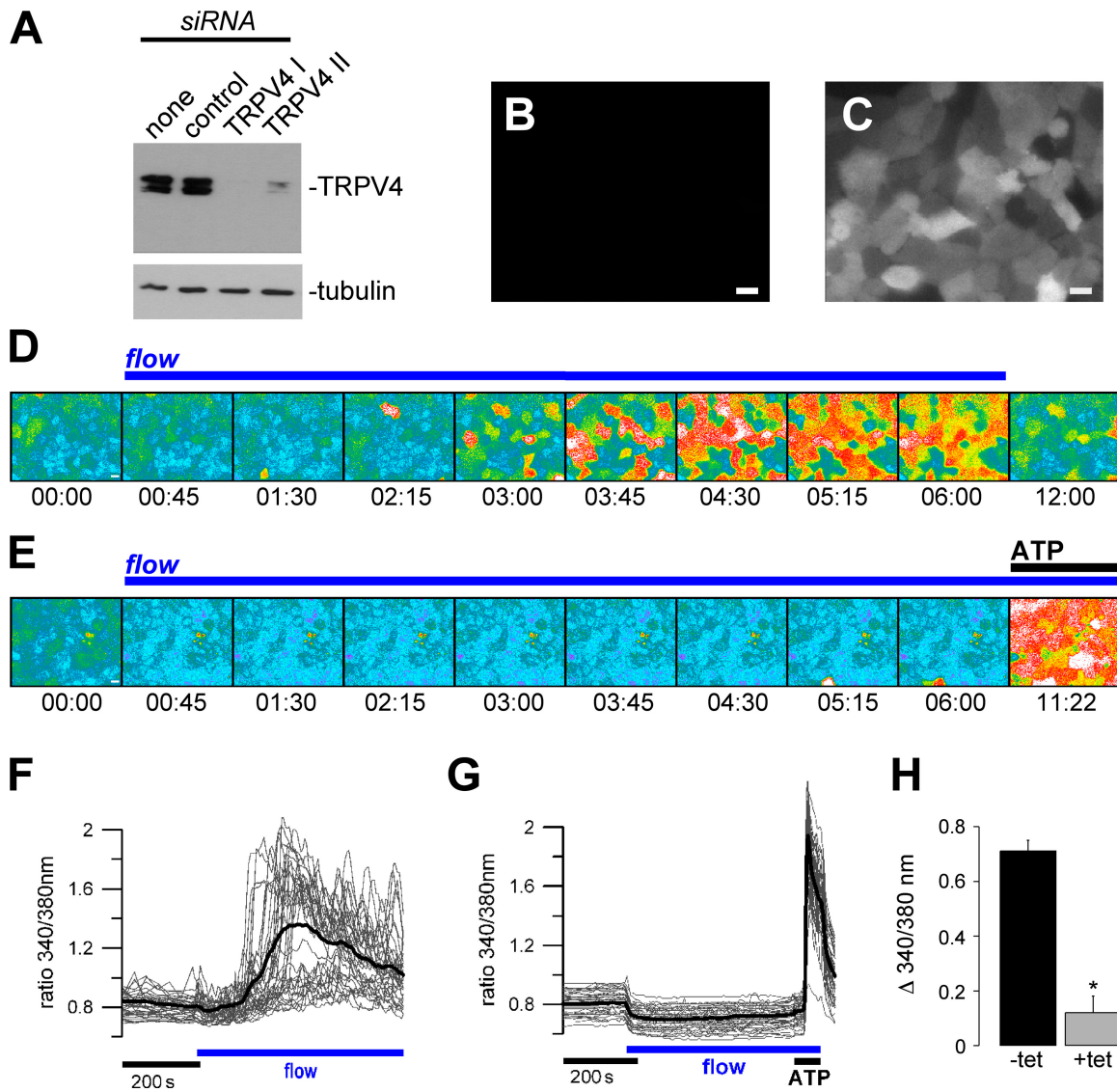


Figure 3. TRPV4 is required for flow-mediated Ca^{2+} signals in renal epithelial cells. (A) HEK 293 cells overexpressing V5-tagged canine TRPV4 were transiently transfected with empty vector (none), an ineffective siRNA construct (control), or two different effective siRNA constructs. TRPV4 expression levels were monitored by Western blotting against V5 (with tubulin as a loading control). (B and C) MDCK cells stably expressing tetracycline-inducible TRPV4 II siRNA. siRNA expression in the absence (B) and presence of tetracycline (C) can be monitored by concomitant expression of GFP. (D) Flow-mediated Ca^{2+} signaling was studied in ciliated MDCK cells using Fura-2. The time course of cytosolic Ca^{2+} increase in response to laminar flow (ciliary bending) is shown in representative Fura-2 pseudocolor images reflecting the Ca^{2+} concentration in MDCK cells (340/380 nm fluorescence ratio; blue/green: low $[\text{Ca}^{2+}]_c$; yellow/red: high $[\text{Ca}^{2+}]_c$; time is indicated in min:s). (E) Flow-induced Ca^{2+} signals in cells expressing TRPV4 siRNA. Although the flow-induced response was abolished upon knockdown of TRPV4, 10 μM ATP still elicited a robust Ca^{2+} increase. (F) Single-cell analysis of the Ca^{2+} signals (ratio 340/380 nm) of the same experiment as shown in D (each trace represents an individual cell and the bold line depicts the mean; for better visibility, only 50% of cells in the visual field are represented). (G) Effect of TRPV4 siRNA on flow-induced Ca^{2+} signals. Single-cell analysis of the same experiment as shown in E; again, 50% of cells in the visual field are represented. (H) Grouped data from three independent experiments ($n = 3$; -tet: 75 cells per n ; +tet: 93 cells per n). All cells in the visual field were included to calculate the flow-induced Ca^{2+} peak baseline. *, statistical significance. Error bars represent mean values \pm SEM. Bars, 10 μm .

for flow-induced Ca^{2+} signals, the lack of renal cysts in TRPV4-deficient animals indicates that activation of the ciliary polycystin-1–TRPP2 complex by a mechanism other than flow-induced deflection of the cilium might be critical for the regulation of tubular morphology.

Materials and methods

Materials

TRPP2 constructs have been described previously (Arnould et al., 1999; Köttgen et al., 2005). The plasmid for mouse TRPV4 was provided by

V. Flockerzi (University of Saarland, Saarbrücken, Germany). The carboxy-terminal TRPV4-GFP fusion was a gift of W. Liedtke (Duke University, Durham, NC). The plasmids psGEM-TRPP2 and psGEM-mTRPV4 for cRNA synthesis and the TRPP2 and TRPV4 constructs fused to fluorescent proteins and epitope tags were generated using standard cloning techniques. The TRPV4-V5 loop with a V5 tag engineered into the first extracellular loop for surface detection has been described previously (Wegierski et al., 2006). Similarly, a V5 tag was engineered into the second extracellular loop of human TRPP2 (TRPP2-V5 loop; in the cdm8 vector). For electrophysiology, Ca^{2+} imaging experiments and expression in zebrafish untagged TRPP2 and TRPV4 constructs were used. All other chemicals were obtained from Sigma-Aldrich. Water-insoluble drugs were dissolved in dimethyl sulfoxide or ethanol (final solvent concentration was <0.1%).

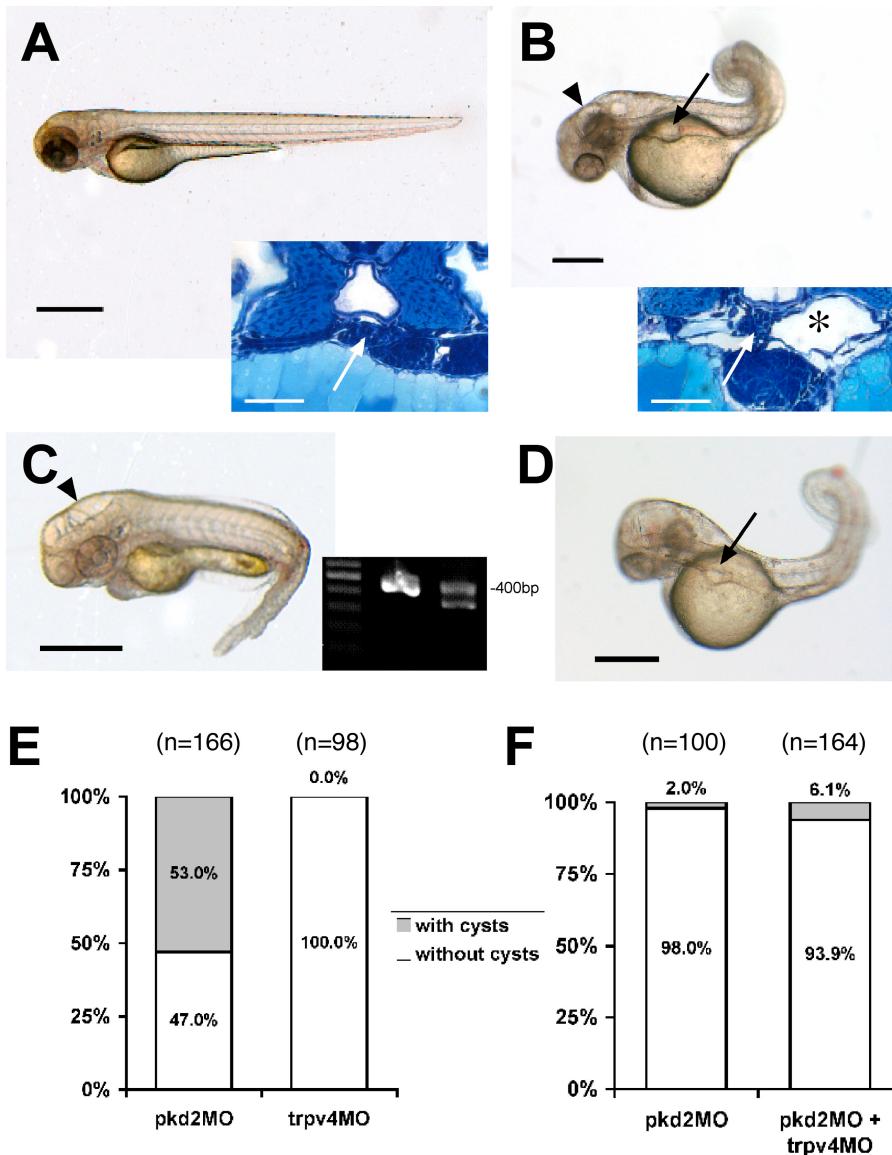


Figure 4. Role of TRPP2 and TRPV4 in the pathogenesis of pronephric cysts in zebrafish. (A) Wild-type larva (55 hpf) with histologically normal glomerulus (inset, arrow) and adjacent tubules. Bars, 500 pm. (B) Disruption of TRPP2 function in *pkd2* morpholino (*pkd2MO*)-injected larva (55 hpf) results in dorsally flexed curly tail, hydrocephalus (arrowhead), and pronephric cyst formation (arrow), which is confirmed histologically. The pronephric tubules are dilated (inset, *) and the glomerulus is stretched (inset, arrow). (C) *trpv4* morphant larva (55 hpf) show hydrocephalus (arrowhead) but lack pronephric cysts (grouped data are shown in E). The effect of the *trpv4* splice morpholino was verified by RT-PCR (inset) from single embryo total RNA (55 hpf), with nested primers in flanking exons yielding a 400-bp amplicon in wild-type embryos (middle lane) and an additional shorter amplicon in the morphant embryo (right lane; 100 bp marker, left lane). Sequencing revealed an in-frame deletion of the whole seventh coding exon (93 bp) and therefore the loss of most of the second transmembrane domain. Higher *trpv4* MO doses led to substantial increase of lethality in the injected embryos. To examine an interaction between the two proteins with respect to cyst formation, the embryos were injected with both morpholinos. (D) With two morpholinos, *pkd2MO* and *trpv4MO*, the coinjected embryo (55 hpf) shows a pronephric cyst (arrow). For the coinjection, the dose of the *pkd2MO* was titrated to levels at which the occurrence of cysts is very low, and *trpv4MO* was added in a medium dose with low lethality. The additive effect showed no significant increase in incidence of cysts, as is shown in the bar graph (F).

Cell culture and transfection

MDCK or HEK 293 cells were grown at 37°C in DME supplemented with 10% heat-inactivated fetal bovine serum. Cells were transfected with Fu-gene 6 (Roche) and calcium phosphate, and experiments were performed 2–5 d after transfection. Transgene expression was monitored by fluorescence detection and Western blot analysis.

RNA interference

Canine TRPV4 was cloned from MDCK cDNA into the HindIII and NotI sites of pCDNA6.V5 and sequenced (GenBank/EMBL/DDBJ accession no. EF561643). The efficacy of TRPV4 siRNA sequences was tested by coexpressing different siRNA-expressing pSuper plasmids with cTRPV4.V5 in HEK 293T cells and testing the amount of cTRPV4.V5 protein by Western blotting. Two siRNAs showing consistent high level suppression of TRPV4 were cloned into pLVTH, which in addition to the H1 promoter carries a EF1α promoter-driven GFP reporter (Wiznerowicz and Trono, 2003). Lentivirus produced with the pLVTH clones was used to transduce MDCK cells expressing the KRAB Tet repressor, which represses both siRNA and GFP expression. TRPV4 I- and TRPV4 II siRNA-transduced MDCK cells were seeded on coverslips at high density and either maintained with or without 5 mg/liter tetracycline for 9–12 d. The induction of siRNA was monitored visually according to GFP expression. siRNA target sequence I: 5'-GGAAGAACGGTCATCGAGAACG-3'; target sequence II: 5'-GGAGGTGACAGATGAGGATAC-3'. A modified target sequence II (TRPV4 IIIm) with a two-base mismatch that does not affect

TRPV4 expression was used as a negative control: 5'-GGAGGTGACA-AACGAGGATAC-3' (Fig. S2).

Immunofluorescence

MDCK cells were grown on 25-mm glass coverslips and processed for indirect immunofluorescence 8–14 d after reaching confluence. Cells were fixed in formaldehyde/PBS and permeabilized in blocking buffer (0.2% Triton X-100 or 100% methanol, and 0.2% goat serum in PBS). Fixed cells were incubated with the following antibodies: mouse anti-acetylated tubulin (Sigma-Aldrich), rabbit anti-TRPV4 (provided by S. Heller, Stanford University School of Medicine, Stanford, CA; Cuajungco et al., 2006), and mouse anti-TRPP2 (D3; Santa Cruz Biotechnology, Inc.). Antibodies were visualized using Alexa 488-labeled anti-rabbit IgG and Alexa 568 anti-mouse antibodies (Invitrogen). Nuclei were stained with DAPI. Images were captured at room temperature using a 63×/1.2 oil immersion objective on a confocal microscope (LSM 510; Carl Zeiss, Inc.) using the LSM 510 software (Carl Zeiss, Inc.). Representative results of at least three independent experiments are shown.

Ca²⁺ imaging and laminar flow chamber

A parallel-plate flow chamber was used as described previously (Kotsis et al., 2007). Laminar flow in the channel was obtained with Ringer solution at 37°C and a physiological flow rate of 0.83 μl/s (linear velocity of 2.0 mm/s) in a thermostatic-controlled, water-driven heating unit mounted on the stage of an inverted microscope (Axiovert 100M; Carl

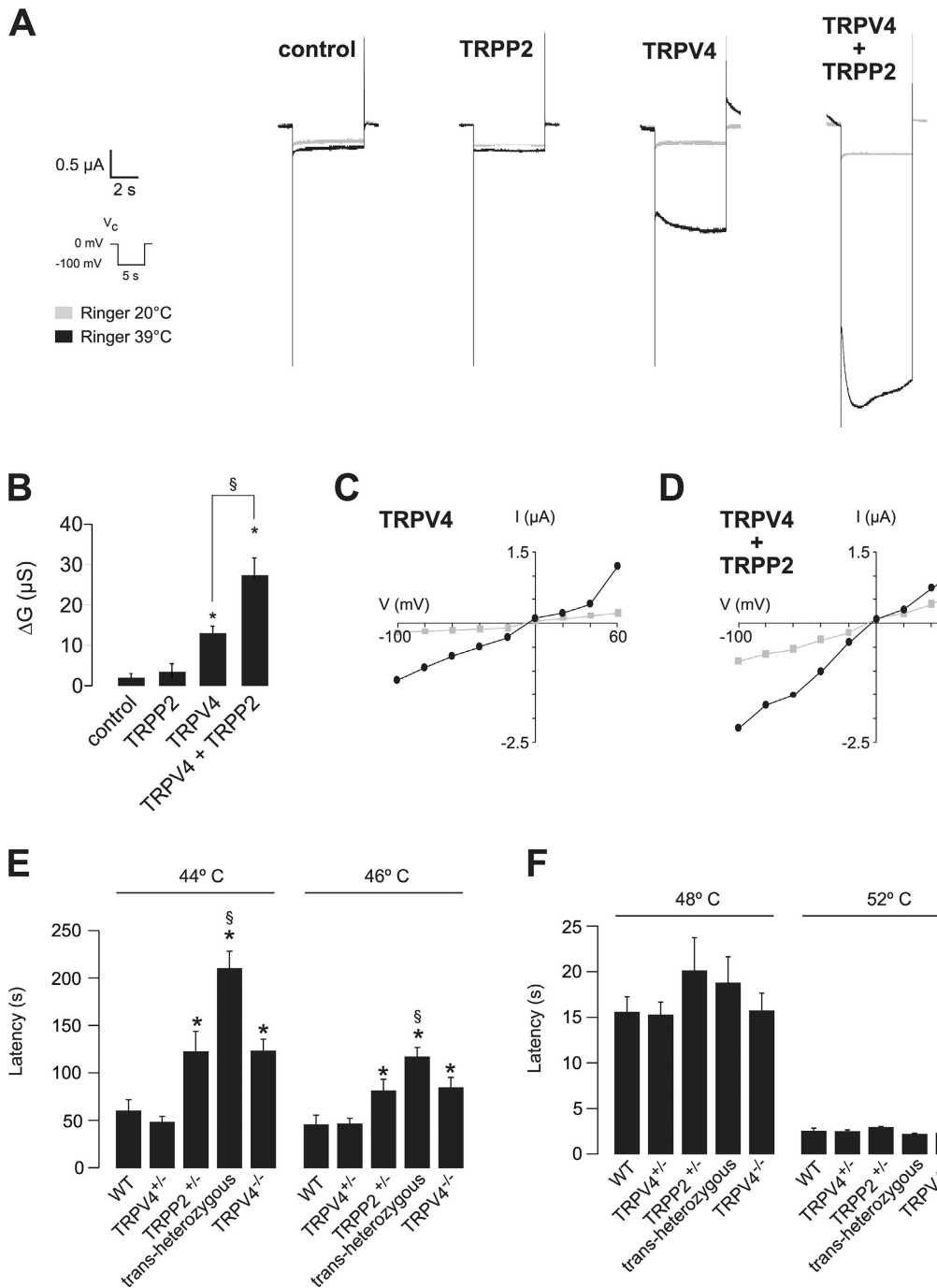


Figure 5. TRPP2 and TRPV4 form a thermosensory complex in vitro and in vivo. (A) Analysis of TRP channel whole-cell currents under voltage clamp (V_c) conditions. Currents were recorded in *X. laevis* oocytes injected with cRNA encoding TRPP2 and/or TRPV4. Representative inward currents at 20°C or 39°C are shown. (B) Summary of data acquired in A. Asterisks indicate significant differences in the temperature-activated whole cell conductance (ΔG) compared with water-injected control oocytes; §, significant differences between data as indicated ($n = 4, 4, 4$, and 6 , respectively). (C) Current-voltage (I - V) relations for oocytes expressing TRPV4 or TRPV4 and TRPP2 (D; gray: 20°C; black: 39°C). (E) Tail withdrawal latencies after immersion into a water bath at moderately hot temperatures were measured in mice of the indicated genotypes ($n = 10$ per genotype; asterisk indicates significant difference compared with wild-type [WT] and TRPV4^{+/−} mice; §, significant difference from TRPP2^{+/−} mice). (F) Tail withdrawal latencies at noxiously hot temperatures ($n = 10$ per genotype). Error bars represent mean values \pm SEM.

Zeiss, Inc.). Cells were incubated with 5 μ M Fura-2 AM in a solution containing 1 mM probenecide for 20–40 min at 37°C. The presence of cilia was demonstrated by differential interference contrast microscopy (Kotsis et al., 2007). The inverted microscope was equipped with a fast-switching monochromator (Cairn Research Limited), a cooled charge-coupled device camera (Coolsnap HQ; Photometrics), and fast shutters in the excitation and transmitted light beam path. A 63 \times /1.2W C-Apochromat lens (Carl Zeiss, Inc.) was used for image acquisition.

Images were recorded with 600–800-ms exposure time at acquisition rates of 2–20/min. Excitation was alternated between 340 nm and 380 nm, and emission was collected by using a filter combination DC430 and BP480-520 (AHF Analysentechnik AG). Experiments were recorded and analyzed with the Metafluor software (MDS Analytical Technologies). For statistical analysis, ratio values for all the cells (66–104) in one field of view were measured, and the mean was referred to as one independent experiment.

Electrophysiology

Two-electrode voltage clamp experiments were performed as described previously (Köttgen et al., 2005). In brief, oocytes were isolated by partial ovariotomy from *X. laevis* frogs. cRNAs were synthesized in vitro using the mMessage mMachine kit (Ambion). Stage V and VI oocytes were injected with 30 nl of water containing 10 ng of TRPP2 and/or TRPV4 cRNA, or water as a control. Voltage clamp experiments were performed 2–5 d after injection of cRNAs. Whole-cell currents of oocytes were recorded using the Turbo TEC O3X amplifier (NPI Electronic GmbH). All whole-cell voltage clamp experiments were performed at 20°C in ND96 frog Ringer (control) solution (96 mM NaCl, 2 mM KCl, 1.8 mM CaCl₂, 1 mM MgCl₂, and 5 mM Hepes; in the hypotonic solution, the NaCl concentration was reduced by 30%). Oocytes were clamped at 0 mV, and voltage ramps from –100 to +50 mV were applied every 1.2 s. Alternatively, voltage steps from 0 mV to –100 mV were applied as indicated. For temperature activation experiments, oocytes were superfused with ND96 at 39°C (control 20°C). Temperature was monitored by a thermometer in the bath chamber. Whole-cell conductance was determined in the voltage range from –100 to 0 mV. Data are presented as original recordings or as mean values ± SEM (*n* = number of experiments).

ELISA for surface detection

HEK 293T cells transfected by the calcium phosphate method were split on the following day into poly-L-lysine-coated 48-well dishes. 2 d after transfection, the cells were fixed with 3.7% paraformaldehyde and blocked with 2% horse serum in PBS. The plasma membrane-localized proteins bearing the extracellular V5 epitope were labeled with mouse anti-V5 (2 µg/ml) and anti-mouse alkaline phosphatase (AP)-coupled antibodies. After three washes with PBS, the enzymatic reaction was performed in 0.1 M glycine, 1 mM MgCl₂, and 1 mM ZnCl₂, pH 10.4, using 1 mg/ml pNitrophenyl phosphate as substrate. The absorbance was read at 405 nm. For each experiment, all conditions were tested in triplicate. The mean absorbance obtained for mock-transfected cells was subtracted as background. In contrast to the TRPV4-V5 loop protein, expression of which stimulated efficient conversion of the AP substrate, the enzymatic reaction on cells expressing TRPP2-V5 loop protein resulted in a modest increase in the amount of AP product as compared with the mock-transfected cells (21% increase on average). Thus, transiently expressed TRPP2 appears not to localize efficiently at the surface of HEK 293T cells. The total amounts of expressed proteins were determined by Western blotting using whole-cell lysates of the transfected cells split in parallel. The blots were scanned and the bands were quantified using ImageJ software (National Institutes of Health). Statistical analysis was performed using a one-sample *t* test.

FRET

Carboxy-terminal fusions of TRPP2 with CFP and TRPV4 with YFP were co-expressed with a cDNA ratio of 1:3 (CFP/YFP) to minimize the probability of CFP-only multimers. Nonconfluent living cells in glass-bottom Petri dishes were examined using a confocal microscope (LSM 510 Meta) with a 63× objective (C-Apochromat 63×/1.2 W), a pixel size of 0.084 µm, and a pixel time of 1.6 µs. For FRET measurements, the spectral Meta detector of the LSM was used with seven channels covering the emission wavelength range from 463–613, with a bandwidth of 20 nm. Channels were recorded simultaneously using only 458-nm excitation. This resulted in an emission signal originating from TRPP2-CFP-alone constructs as well as TRPP2-CFP/TRPV4-YFP FRET pairs, and to a minor extent from TRPV4-YFP. The use of 458-nm excitation only strongly reduced the excitation of the TRPV4-YFP constructs. After nine excitation cycles (every 5 s) with 458-nm excitation used as baseline intensity values, five excitation cycles with an additional photobleach pulse with 514 nm (maximum laser power) followed, then 458-nm-only excitation cycles were used until a total recording time of 100 s was reached. This procedure resulted in >90% of YFP photobleached within <40 s. The signal of the seven emission channels was spectrally unmixed into the CFP- and YFP-related components using the LSM 510 software and reference spectra recorded at identical recording conditions from TRPP2-CFP- and TRPV4-YFP-only transfected cells as well as background correction. The unmixing process resulted in two images containing the unmixed CFP and YFP signals and a third channel containing residual signal, which could not be accounted to CFP or YFP. We quantified the percentage change of CFP (donor) or YFP (acceptor) fluorescence after bleach of the acceptor, YFP. The maximal CFP signal or YFP signal reached during any time point of the single experiment was used as the 100% reference value.

Western blotting

Western blot analysis and coimmunoprecipitations were performed as described previously (Arnould et al., 1999; Köttgen et al., 2005). In brief, 24 h after transfection, cells were lysed in 1 ml/10 cm dish of ice-cold lysis buffer

(1% Triton X-100, 20 mM Tris-HCl, pH 7.5, 50 mM NaCl, 50 mM NaF, 15 mM Na₄P₂O₇, 2 mM Na₃VO₄, and protease inhibitors) for 15 min on ice. Lysates were centrifuged at 4°C for 15 min at 14,000 rpm. Supernatants were used for Western blotting and coimmunoprecipitation studies. Representative results of at least three independent experiments are shown.

Zebrafish experiments

Morpholino antisense oligonucleotides were designed to target an exon splice donor site causing splicing defects of the mRNA. The MOs were obtained from Gene Tools, LLC. The following morpholinos were used: *pkd2MO* (5'-AATTACTTCCAGAACGCTCCATG-3'; Obara et al., 2006) targeting the splice donor of the third exon coding for part of the first transmembrane domain and part of the first extracellular loop, and *trpv4MO* (5'-GTTACAAAGAAAAAGAGTCCAGAAC-3') targeting the splice donor of the seventh coding exon coding for the second transmembrane domain. The morpholinos for single and double injections were diluted in 100 mmol/liter KCl, 10 mmol/liter Hepes, and 0.1% Phenol red (Sigma-Aldrich). The injections were performed using a microprocessor-controlled nanoliter injector (Nanoliter 2000; World Precision Instruments, Inc.) under stereomicroscopic control (MZ16; Leica). The effect of the *trpv4* splice morpholino was verified by RT-PCR from single embryo total RNA with nested primers in flanking exons.

Embryos were fixed in BT-Fix at 4°C overnight (Westerfield, 2000). After being washed in PBS and taken through an ethanol dehydration series, they were embedded in Technovit 7100 resin (Heraeus Kulzer) and sectioned at 5 µm. Slides were stained in methyleneblue/azure II (Humphrey and Pittman, 1974), mounted, and examined using an Axiovert microscope (Carl Zeiss, Inc.).

Total RNA from single embryos was obtained by using an RNeasy kit (QIAGEN). The zebrafish *trpv4* sequence was derived partially by TBLASTN searches (Sanger Institute, Cambridge, UK). Part of the coding sequence was obtained by reverse transcription and nested PCR of wild-type total RNA (outer primer set: forward, 5'-TTCCAGCAGGGTTTTCTGCTTCC-3'; reverse, 5'-TCTCCCCCATCAGAGCGATAACA-3'; nested primer set: forward, 5'-ATCGTCTGGCCATGACAGAGTCCT-3'; reverse, 5'-AGAATGAG-GAAGACGGCGGATAC-3') and subcloned into pCRII using TA cloning (Invitrogen). The morpholino effect was verified by RT-PCR using the following set of primers: outer primer pair forward (5'-TGGGCTTATGGACCAGT-GTACTCC-3') and reverse (5'-AAAGCAAACACCATCACAGACACG-3'), and inner primer pair forward (5'-ACCTGCGGAGAGGAAGTGTCTGTT-3') and reverse (5'-GGCCTCAATGCCTGACAGATACAG-3').

Tail immersion assay in mice

TRPV4 knockout mice (Suzuki et al., 2003) were backcrossed five generations onto a C57BL/6 background. TRPP2 conditional knockout mice were generated by homologous recombination using standard techniques. In brief, a loxP site was inserted in intron 10 of *Pkd2* and a loxP-FRT-PGKneo-FRT cassette in intron 13 (*Pkd2^{2m1Tm}*). After removal of Pgkneo, Cre-mediated recombination (*B6.129S4-Meo2^{2m1cre}Sor/J*; the Jackson Laboratory) between the loxP sites was predicted to result in loss of the carboxy-terminal tail of the protein (*Pkd2^{2m1Tm}*). Animals of different genotypes were obtained by mating of TRPP2^{+/−} animals with TRPV4^{+/−} or TRPV4^{−/−} animals, and genotypes were determined by PCR. Age-matched male mice 11–17 wk of age were individually housed at least 1 h before behavioral assays. Ambient temperature was maintained at 25 ± 1°C, with a light cycle from 8:00 a.m. to 8:00 p.m. All behavioral assays were performed between 12 p.m. and 8 p.m. A single cohort of animals was used in all experiments. All experiments were conducted according to protocols approved by The Johns Hopkins Animal Care and Use Committee.

The tail immersion assays were performed as described previously (Lee et al., 2005). After a 30-min acclimation in a Plexiglas box, the tail of a gently restrained mouse was immersed in a water bath set at a single temperature from 44–52°C, and the time to tail flick was recorded. This assay was performed with the investigator blinded to genotype. Latencies at a given temperature were recorded during three trials separated by at least 1 d and averaged. Mice were allowed to rest at least 1 d between temperatures. The cutoff time was 300 s, after which the tail was removed from the bath regardless of response.

Statistical analysis

Data are presented as original recordings or as mean values ± SEM (*n* = number of experiments). Unpaired and paired *t* tests as applicable were used for statistical analysis. A *p*-value of <0.05 was accepted to indicate statistical significance. For zebrafish experiments, a stratified χ^2 test (Cochran-Mantel-Haenszel test) was used, and a *p*-value of <0.05 was accepted to indicate statistical significance.

Online supplemental material

Fig. S1 shows subcellular localization of native and overexpressed TRPV4 in polarized MDCK cells and FRET negative controls. Fig. S2 shows that flow-mediated Ca^{2+} signals are inhibited by RR and are not affected in cells expressing a two-base mismatch TRPV4 siRNA. Fig. S3 shows the functional interaction of TRPP2 and TRPV4 in HEK 293 cells. Online supplemental material is available at <http://www.jcb.org/cgi/content/full/jcb.200805124/DC1>.

We are grateful to N. Katsanis for sharing unpublished information and V. Flockerzi, S. Heller, and W. Liedtke for plasmids and antibodies. We thank M. Caterina for discussions and support with the TRPV4 knockout animals, and Emily Kim for helpful suggestions.

This work was supported by the Deutsche Forschungsgemeinschaft (support given to G. Walz), a PKD Foundation Fellowship (to M. Köttgen), the National Kidney Foundation of Maryland, Inc. (grant GM073704 to T. Watnick), the Human Frontiers Science Program (grant RGP 32/2004 to B. Nilius) and Excellentie financiering (grant EF/95/010 to B. Nilius), and the National Institutes of Health (grants DK48006 and DK51259 to G.G. Germino).

Submitted: 20 May 2008

Accepted: 7 July 2008

Note added in proof. A recent study from Bai et al. (Bai, C.X., A. Giamarchi, L. Rodat-Despoix, F. Padilla, T. Downs, L. Tsikas, and P. Delmas. 2008. *EMBO Rep.* 9:472–479) reports the heteromeric assembly of TRPP2 and TRPC1 subunits.

References

- Arnould, T., L. Sellin, T. Benzing, L. Tsikas, H.T. Cohen, E. Kim, and G. Walz. 1999. Cellular activation triggered by the autosomal dominant polycystic kidney disease gene product PKD2. *Mol. Cell. Biol.* 19:3423–3434.
- Cuajungco, M.P., C. Grimm, K. Oshima, D. D’Hoedt, B. Nilius, A.R. Mensenkamp, R.J. Bindels, M. Plomann, and S. Heller. 2006. PACSINs bind to the TRPV4 cation channel. PACSIN 3 modulates the subcellular localization of TRPV4. *J. Biol. Chem.* 281:18753–18762.
- Giamarchi, A., F. Padilla, B. Coste, M. Raoux, M. Crest, E. Honore, and P. Delmas. 2006. The versatile nature of the calcium-permeable cation channel TRPP2. *EMBO Rep.* 7:787–793.
- Gradilone, S.A., A.I. Masyuk, P.L. Splinter, J.M. Banales, B.Q. Huang, P.S. Tietz, T.V. Masyuk, and N.F. Larusso. 2007. Cholangiocyte cilia express TRPV4 and detect changes in luminal tonicity inducing bicarbonate secretion. *Proc. Natl. Acad. Sci. USA.* 104:19138–19143.
- Guler, A.D., H. Lee, T. Iida, I. Shimizu, M. Tominaga, and M. Caterina. 2002. Heat-evoked activation of the ion channel, TRPV4. *J. Neurosci.* 22:6408–6414.
- Hanaoka, K., F. Qian, A. Boletta, A.K. Bhunia, K. Piontek, L. Tsikas, V.P. Sukhatme, W.B. Guggino, and G.G. Germino. 2000. Co-assembly of polycystin-1 and -2 produces unique cation-permeable currents. *Nature.* 408:990–994.
- Hidaka, S., V. Konecke, L. Osten, and R. Witzgall. 2004. PIGEA-14, a novel coiled-coil protein affecting the intracellular distribution of polycystin-2. *J. Biol. Chem.* 279:35009–35016.
- Humphrey, C.D., and F.E. Pittman. 1974. A simple methylene blue-azure II-basic fuchsin stain for epoxy-embedded tissue sections. *Stain Technol.* 49:9–14.
- Kahn-Kirby, A.H., and C.I. Bargmann. 2006. TRP channels in *C. elegans*. *Annu. Rev. Physiol.* 68:719–736.
- Kim, K., I. Drummond, O. Ibraghimov-Beskrovnaya, K. Klinger, and M.A. Arnalout. 2000. Polycystin 1 is required for the structural integrity of blood vessels. *Proc. Natl. Acad. Sci. USA.* 97:1731–1736.
- Kotsis, F., R. Nitschke, C. Boehlke, M. Bashkurov, G. Walz, and E.W. Kuehn. 2007. Ciliary calcium signaling is modulated by kidney injury molecule-1 (Kim1). *Pflugers Arch.* 453:819–829.
- Köttgen, M. 2007. TRPP2 and autosomal dominant polycystic kidney disease. *Biochim. Biophys. Acta.* 1772:836–850.
- Köttgen, M., and G. Walz. 2005. Subcellular localization and trafficking of polycystins. *Pflugers Arch.* 451:286–293.
- Köttgen, M., T. Benzing, T. Simmen, R. Tauber, B. Buchholz, S. Feliciangeli, T.B. Huber, B. Schermer, A. Kramer-Zucker, K. Hopker, et al. 2005. Trafficking of TRPP2 by PACS proteins represents a novel mechanism of ion channel regulation. *EMBO J.* 24:705–716.
- Lee, H., T. Iida, A. Mizuno, M. Suzuki, and M.J. Caterina. 2005. Altered thermal selection behavior in mice lacking transient receptor potential vanilloid 4. *J. Neurosci.* 25:1304–1310.
- Liedtke, W., and J.M. Friedman. 2003. Abnormal osmotic regulation in trpv4^{-/-} mice. *Proc. Natl. Acad. Sci. USA.* 100:13698–13703.
- Liedtke, W., Y. Choe, M.A. Marti-Renom, A.M. Bell, C.S. Denis, A. Sali, A.J. Hudspeth, J.M. Friedman, and S. Heller. 2000. Vanilloid receptor-related osmotically activated channel (VR-OAC), a candidate vertebrate osmo-receptor. *Cell.* 103:525–535.
- Liedtke, W., D.M. Tobin, C.I. Bargmann, and J.M. Friedman. 2003. Mammalian TRPV4 (VR-OAC) directs behavioral responses to osmotic and mechanical stimuli in *Caenorhabditis elegans*. *Proc. Natl. Acad. Sci. USA.* 100(Suppl 2):14531–14536.
- Liu, W., N.S. Murcia, Y. Duan, S. Weinbaum, B.K. Yoder, E. Schwiebert, and L.M. Satlin. 2005. Mechanoregulation of intracellular Ca^{2+} concentration is attenuated in collecting duct of monocilia-impaired orpk mice. *Am. J. Physiol. Renal Physiol.* 289:F978–F988.
- Lu, W., and J. Zhou. 1997. Perinatal lethality with kidney and pancreas defects in mice with a targeted Pkd1 mutation. *Nat. Genet.* 17:179–181.
- Mangos, S., Y. Liu, and I.A. Drummond. 2007. Dynamic expression of the osmo-sensory channel trpv4 in multiple developing organs in zebrafish. *Gene Expr. Patterns.* 7:480–484.
- Mizuno, A., N. Matsumoto, M. Imai, and M. Suzuki. 2003. Impaired osmotic sensation in mice lacking TRPV4. *Am. J. Physiol. Cell Physiol.* 285:C96–C101.
- Nauli, S.M., F.J. Aleghat, Y. Luo, E. Williams, P. Vassilev, X. Li, A.E. Elia, W. Lu, E.M. Brown, S.J. Quinn, et al. 2003. Polycystins 1 and 2 mediate mechanosensation in the primary cilium of kidney cells. *Nat. Genet.* 33:129–137.
- Nilius, B., J. Prenen, U. Wissenbach, M. Bodding, and G. Droogmans. 2001. Differential activation of the volume-sensitive cation channel TRP12 (OTRPC4) and volume-regulated anion currents in HEK-293 cells. *Pflugers Arch.* 443:227–233.
- Nilius, B., J. Vriens, J. Prenen, G. Droogmans, and T. Voets. 2004. TRPV4 calcium entry channel: a paradigm for gating diversity. *Am. J. Physiol. Cell Physiol.* 286:C195–C205.
- Obara, T., S. Mangos, Y. Liu, J. Zhao, S. Wiessner, A.G. Kramer-Zucker, F. Olale, A.F. Schier, and I.A. Drummond. 2006. Polycystin-2 immunolocalization and function in zebrafish. *J. Am. Soc. Nephrol.* 17:2706–2718.
- Ong, A.C., and D.N. Wheatley. 2003. Polycystic kidney disease—the ciliary connection. *Lancet.* 361:774–776.
- Prætorius, H.A., and K.R. Spring. 2001. Bending the MDCK cell primary cilium increases intracellular calcium. *J. Membr. Biol.* 184:71–79.
- Schaefer, M. 2005. Homo- and heteromeric assembly of TRP channel subunits. *Pflugers Arch.* 451:35–42.
- Sun, Z., A. Amsterdam, G.J. Pazour, D.G. Cole, M.S. Miller, and N. Hopkins. 2004. A genetic screen in zebrafish identifies cilia genes as a principal cause of cystic kidney. *Development.* 131:4085–4093.
- Suzuki, M., A. Mizuno, K. Kodaira, and M. Imai. 2003. Impaired pressure sensation in mice lacking TRPV4. *J. Biol. Chem.* 278:22664–22668.
- Tan, P.L., T. Barr, P.N. Inglis, N. Mitsuma, S.M. Huang, M.A. Garcia-Gonzalez, B.A. Bradley, S. Coforio, P.J. Albrecht, T. Watnick, et al. 2007. Loss of Bardet Biedl syndrome proteins causes defects in peripheral sensory innervation and function. *Proc. Natl. Acad. Sci. USA.* 104:17524–17529.
- Taniguchi, J., S. Tsuruoka, A. Mizuno, J. Sato, A. Fujimura, and M. Suzuki. 2007. TRPV4 as a flow sensor in flow-dependent K^+ secretion from the cortical collecting duct. *Am. J. Physiol. Renal Physiol.* 292:F667–F673.
- Teilmann, S.C., A.G. Byskov, P.A. Pedersen, D.N. Wheatley, G.J. Pazour, and S.T. Christensen. 2005. Localization of transient receptor potential ion channels in primary and motile cilia of the female murine reproductive organs. *Mol. Reprod. Dev.* 71:444–452.
- Tian, W., M. Salanova, H. Xu, J.N. Lindsley, T.T. Oyama, S. Anderson, S. Bachmann, and D.M. Cohen. 2004. Renal expression of osmotically responsive cation channel TRPV4 is restricted to water-impermeant nephron segments. *Am. J. Physiol. Renal Physiol.* 287:F17–F24.
- Tobin, D., D. Madsen, A. Kahn-Kirby, E. Peckol, G. Moulder, R. Barstead, A. Maricq, and C. Bargmann. 2002. Combinatorial expression of TRPV channel proteins defines their sensory functions and subcellular localization in *C. elegans* neurons. *Neuron.* 35:307–318.
- Todaka, H., J. Taniguchi, J.I. Satoh, A. Mizuno, and M. Suzuki. 2004. Warm temperature-sensitive TRPV4 plays an essential role in thermal hyperalgesia. *J. Biol. Chem.* 279:35133–35138.
- Torres, V.E., and P.C. Harris. 2006. Mechanisms of disease: autosomal dominant and recessive polycystic kidney diseases. *Nat. Clin. Pract. Nephrol.* 2:40–55.
- Tsikas, L., T. Arnould, C. Zhu, E. Kim, G. Walz, and V.P. Sukhatme. 1999. Specific association of the gene product of PKD2 with the TRPC1 channel. *Proc. Natl. Acad. Sci. USA.* 96:3934–3939.
- Voets, T., J. Prenen, J. Vriens, H. Watanabe, A. Janssens, U. Wissenbach, M. Bodding, G. Droogmans, and B. Nilius. 2002. Molecular determinants of permeation through the cation channel TRPV4. *J. Biol. Chem.* 277:33704–33710.
- Watanabe, H., J. Vriens, S.H. Suh, C.D. Benham, G. Droogmans, and B. Nilius. 2002. Heat-evoked activation of TRPV4 channels in a HEK293 cell

- expression system and in native mouse aorta endothelial cells. *J. Biol. Chem.* 277:47044–47051.
- Wegierski, T., K. Hill, M. Schaefer, and G. Walz. 2006. The HECT ubiquitin ligase AIP4 regulates the cell surface expression of select TRP channels. *EMBO J.* 25:5659–5669.
- Westerfield, M. 2000. The Zebrafish Book: A Guide for the Laboratory Use of Zebrafish (*Danio rerio*). Fourth Edition. University of Oregon Press, Eugene, OR, pp. 1.1–10.22.
- Wiznerowicz, M., and D. Trono. 2003. Conditional suppression of cellular genes: lentivirus vector-mediated drug-inducible RNA interference. *J. Virol.* 77:8957–8961.
- Wu, G., V. D'Agati, Y. Cai, G. Markowitz, J.H. Park, D.M. Reynolds, Y. Maeda, T.C. Le, H. Hou Jr., R. Kucherlapati, et al. 1998. Somatic inactivation of Pkd2 results in polycystic kidney disease. *Cell*. 93:177–188.
- Wu, L., X. Gao, R.C. Brown, S. Heller, and R.G. O'Neil. 2007. Dual role of the TRPV4 channel as a sensor of flow and osmolality in renal epithelial cells. *Am. J. Physiol. Renal Physiol.* 293:F1699–F1713.